論文 / 著書情報
Article / Book Information

Title	Proposal and Prototyping of Self-Excited Pneumatic Actuator Using Automatic-Flow-Path-Switching-Mechanism
Authors	Kosuke Tani, Hiroyuki Nabae, Gen Endo, Koichi Suzumori
Citation	IEEE Robotics and Automation Letters (RAL), Vol. 5, Issue 2, pp. 3058-3065
Pub. date	2020, 2
Copyright	(c) 2020 IEEE. Personal use of this material is permitted. Permission from IEEE must be obtained for all other uses, in any current or future media, including reprinting/republishing this material for advertising or promotional purposes, creating new collective works, for resale or redistribution to servers or lists, or reuse of any copyrighted component of this work in other works.
DOI	https://dx.doi.org/10.1109/LRA.2020.2974448
Note	This file is author (final) version.

Proposal and Prototyping of Self-excited Pneumatic Actuator Using Automatic-Flow-Path-Switching-Mechanism

Kosuke Tani[1], Hiroyuki Nabae[1], Gen Endo[1], and Koichi Suzumori[1]

***Abstract*—Robots currently have a wide range of practical applications. However, their widespread use is limited by long design and manufacturing times as well as increasingly complex drive system electronics and software, which have led to high development costs. Therefore, simpler manufacturing, driving, and control methods are required. In this study, we design a pneumatic actuator drive system that combines the printing technique and self-excited vibration. In the proposed actuator, a mechanism for automatically switching the airflow path is used to induce self-excited vibration. Moreover, the actuator is integrally molded by a 3D printer; therefore, no assembly process is required. This actuator can be used to easily build robots in a short time, contributing to more widespread use of robots. In this study, we also calculate the theoretical value of the moving frequency by modeling the actuator and verify the validity of this value through experiments using a prototype actuator. Based on the results, we were able to freely design the operating frequency of the actuator; by using this knowledge, we designed a flapping robot. The robot is also integrally molded by a 3D printer. Finally, we validate its motion through experiments, in order to illustrate one of the many applications of the proposed actuator.**

***Index Terms*—Hydraulic/Pneumatic Actuators, Additive Manufacturing, Mechanism Design**

I. INTRODUCTION

RECENTLY, robots have begun to play an active role in various fields, such as inspecting disaster areas[1] and in surgeries[2]. However, generally applicable robots are not only time consuming to design and manufacture but the electronic circuits and software comprising the drive systems are highly complex. Such high development costs are one of the factors limiting the more widespread use of robots; thus, simpler manufacturing methods, drive systems, and control methods are required.

The use of 3D printing technology has previously been investigated to simplify the robot manufacturing method. By easily molding even complex shapes in a short amount of time, the production costs for robots can be significantly reduced. Moreover, the formation of robot and actuator structures by 3D printing can simplify the manufacturing process; for example, by printing actuators on film-like materials[3][4], ionic polymer-metal composites[5], and printing resin[6][7][8]. However, all of these techniques require assembly after molding and do not allow for a single molding process. Although research on integrated 3D printing of robots have been conducted[9][10], the driving system is complicated.

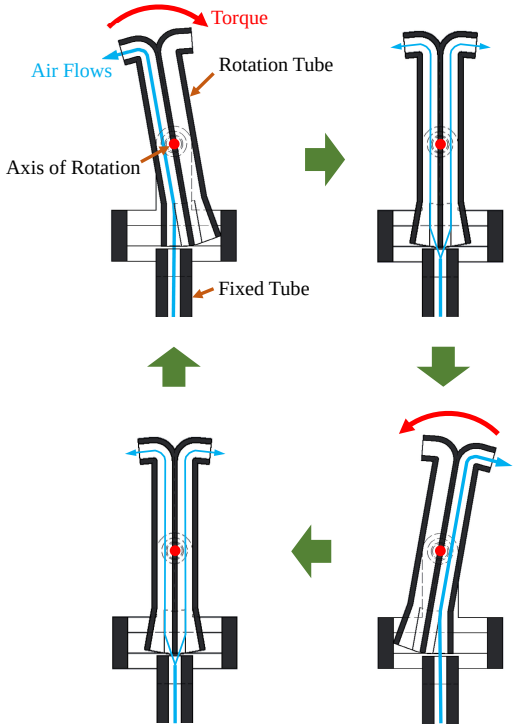

Fig. 1: Operation principle of the proposed actuator. A reciprocating motion is generated by automatically switching a freely rotating pipe arranged in the center of the actuator.

One way to simplify robot drive and control systems is to use self-excited vibration, which produces large movements with a simple structure and control method. It reduces the size of the robots and improves the efficiency of the control methods. More importantly, self-excited vibration can induce vibration without any vibration inputs, leading to simplification of the robot structure. Vibration drive methods without self-excited vibration[11][12][13] require an external device to generate vibration input and the drive system is complicated. Previous examples of self-excited actuators include those that induce vibrations by electrostatic forces[14] or metal deformation due to heat[15], and those using link

Manuscript received: 09, 10, 2019; Revised 12, 20, 2019; Accepted 01, 19, 2020.

This paper was recommended for publication by Editor Paolo Rocco upon evaluation of the Associate Editor and Reviewers' comments.

[1]All authors are with the Department of Mechanical Engineering, Tokyo Institute of Technology, 2-12-1 Ookayama, Meguro-ku, Tokyo 152-8552, Japan nabae@mes.titech.ac.jp

Digital Object Identifier (DOI): see top of this page.

mechanism or unbalanced rotating mass with electromagnetic motor[16][17][18] or with gravity[19][20][21]. However, the mechanism for inducing vibrations is complicated and multiple parts and materials are required. Therefore, they are not suitable for integral molding with 3D printers. Those using chemical reactions[22] have a simple mechanism, but they require the preparation of adequate environments. In contrast, the mechanism of valves[23][24] and robots[25][26] that induce self-excited vibrations by air pressure is relatively simple. In addition, the application of air pressure is characterized by safety to humans and the environment and ensures excellent explosion-proof properties. Therefore, it is expected to play an active role in various situations. In addition, air compressors are generally widely used and are characterized by easy access to energy sources. However they also consist of multiple parts including magnetic materials and are not suitable for integral molding with 3D printers. A previous study realized the same function without the need for elements such as magnets[27], but it still employs an assembly process instead of integral molding. If the actuator consists of a single material, it has been confirmed that pneumatic actuator is more suitable for integrated molding using a 3D printer[28].

Therefore, this study designs and develops an actuator that combines integral molding by 3D printing and a drive system based on self-excited vibration. First, we explain the operating principle and design of the prototype actuator. Then, we calculate the theoretical value of the operating frequency by modeling the actuator and verify its validity through experiments with prototype actuators. Finally, we build a flapping robot as an example of the applications of the actuator and confirm its performance through experiments.

II. Operating Principle of the Proposed Actuator

The mechanism that induces self-excited vibration by air has been studied in the field of Fluidics[29][30][31]. However, producing a large motion with an actuator is difficult because most of its mechanism is only for changing the flow path[32]. Therefore, we have devised an operating principle that generates movement when the flow path is switched. The proposed actuator consists of two parts: a fixed tube and a rotation tube. In this novel mechanism, when air pressure is applied to the fixed tube, the rotating tube attached to the center rotates and the flow path automatically switches. This induces self-excited vibration and produces actuator movement. This phenomenon can be treated as self-excited vibration because the angle of the oscillating tube is obtained as output when non-vibrating air input is applied. A schematic diagram is shown in Fig. 1. The tip of the rotary tube is bent at approximately 90° and torque is generated in the rotating tube when the pipe receives the change in momentum when the jet is bent. The rotating tube then rotates due to the generated torque. We assumed that the optimal angle meets the following condition; the angle between the jet direction and the line connecting the center of rotation and the tip of the bent tube is 90°. However, this angle depends on the length of the rotating tube l, so in order to align experimental conditions other than l and I, the values were set to 95°, which is close to that. When the rotating

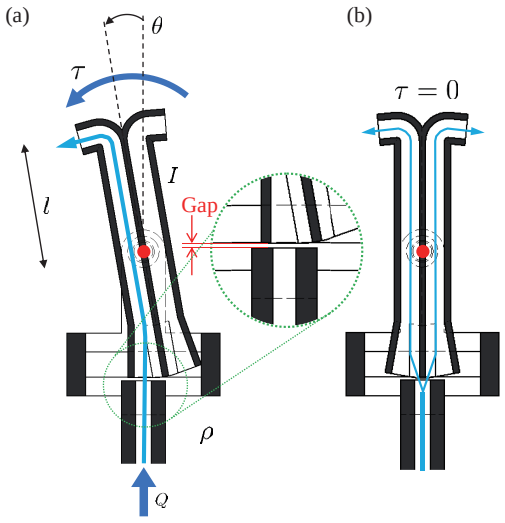

Fig. 2: Description of each value. (a) Situation where the magnitude of the generated torque τ is maximum. (b) Situation where the torques generated in both pipes cancel each other out and $\tau = 0$.

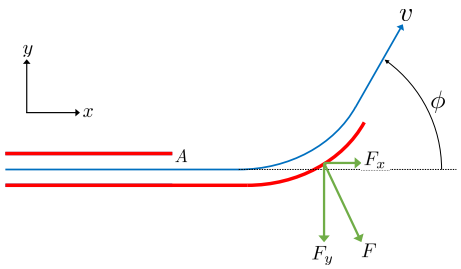

Fig. 3: Model of one side of the rotating tube. The flow path bent by the pipe is modeled as a jet that collides with the curved surface.

tube moves to the center, the generated torques in both tubes cancel each other out and become zero; however, the tube continues to rotate due to inertia. When it reaches the other side, air flows into the other pipe, and torque is generated in the opposite direction by the same principle. By repeating this process, the rotating tube reciprocates. This operation principle can be applied even if there are multiple pipes in the rotating tube. Thus, multiple applications are expected.

III. Theoretical Model and Motion Frequency

We construct a theoretical model of the actuator and derive a theoretical value for its operating frequency.

First, we set the torque and rotation angle when air flows into the actuator at a flow rate of $Q\,[\mathrm{m}^3/\mathrm{s}]$ and a flow velocity of $v\,[\mathrm{m}/\mathrm{s}]$ as Fig. 2. The air density is $\rho\,[\mathrm{kg}/\mathrm{m}^3]$. Let the moment of inertia of the rotating tube be $I\,[\mathrm{kg}\cdot\mathrm{m}^2]$ and the rotation angle of the rotating tube be θ. The rotation range of the rotation angle is then $\theta_{\min} \leq \theta \leq \theta_{\max}$ ($|\theta_{\min}| = |\theta_{\max}|$). When air flows into the tube, torque is generated when it is bent at the tip, and the air velocity that blows into one of the tubes collides with a curved surface with an angle ϕ as

shown in Fig. 3 and a cross-sectional area $A[\mathrm{m}^2]$, representing a two-dimensional jet model. Let $\boldsymbol{F} = (F_x, F_y)$ be the force generated by the impinging jet on the curved surface. There is a gap between the fixed tube and the rotation tube, but the two tubes have the same flow rate. Furthermore, it has been experimentally shown that the operating frequency of the actuator does not change with the gap distance, which will be explained in the next section.

First, the equation of motion of the rotating tube is expressed as shown in Equation(1).

$$I\ddot{\theta} = \tau \tag{1}$$

Here, τ can be expressed by a linear function of the rotation angle θ. The maximum size is realized when $\theta = \theta_{\min}, \theta_{\max}$, and the figure (b) of Fig. 2 describes the situation when $\theta = 0$. As shown in Fig. 2, the torque generated in both pipes cancels out such that $\tau = 0$. From this, Equation (2) can be assumed using a certain value K. The equation of motion is shown in Equation (3).

$$\tau = -K\theta \tag{2}$$

$$I\ddot{\theta} = -K\theta \tag{3}$$

Here, in order to obtain K, we consider the case of $\theta = \theta_{\max}$ when the size of τ is maximized. First, when considering air blown into the tube of one pipe, the equation of momentum in the x-direction and y-direction is given by the following formula.

$$\rho Q\left(v\cos\phi - v\right) = -F_x \tag{4}$$

$$\rho Q v \sin\phi = -F_y \tag{5}$$

Here, $\phi = \pi/2$ is used to obtain the y direction of the force involved in the torque of the rotary tube. Note that the x direction also contributes to the generation of torque, but it was ignored because it was small enough in the y direction.

$$F_y = -\rho Q v \tag{6}$$

$$= -\rho(Av)v \tag{7}$$

$$= -\rho A v^2 \tag{8}$$

K can be obtained using the distance from the rotation axis of the rotating tube to the spout l and equation(8).

$$K = \frac{\rho A l}{\theta_{\max}} v^2 \tag{9}$$

Thus, K can be expressed as a function of v. According to Equation(3),(9), the frequency of motion of the actuator is as follows.

$$f = \frac{1}{2\pi}\sqrt{\frac{\rho A l}{I\theta_{\max}}}\, v \ [\mathrm{Hz}] \tag{10}$$

The frequency is expressed as a linear function of the flow velocity v. The maximum torque of the actuator is described by $\theta = \theta_{\max}$ and in the following equation.

$$\tau_{\max} = \rho A l v^2 \tag{11}$$

Using Equation(10), the operating frequency of the actuator can be designed according to its specific purpose by changing the dimensions of the rotating tube. For example, when the length l of the rotating tube is increased, the operating frequency decreases because the effect of the inertia moment I becomes large. The operating frequency can also be increased by increasing the cross-sectional area A of the rotating tube.

IV. Prototype of the Actuator and Validation Experiments

This section describes the prototype actuator and the experiments conducted to measure the operating frequency of the two-pipe model, which is the basic structure of the actuator and compare it with calculated theoretical values. It shows the validity of the model constructed in the previous section.

A. Prototype actuator

Fig. 4 shows the prototype actuator. This model is the most basic structure of the proposed actuator. We made six models with different gap between two tubes, distances from the center of rotation to the tip l, and the moment of inertia of the rotating tube I. The models were developed with fixed parameters, except for the most important parameters I and l, when designing. Therefore, the inner diameter of all the pipes is 3 mm. This is because it is suitable for experimental conditions including a flow meter. We also developed an extension of the actuator in Fig. 4, as shown in Fig. 5, where the number of pipes was changed to 4 and 10. This extended model operates on the same principle as the two-pipe model. It was shown that the movement of the actuator can be changed by increasing the number of pipes, and the motion trajectory can be mechanically designed. As a result, it can be applied to walking and swimming robots with leg trajectory designs. In addition, the 4-pipe and 10-pipe models do not include a state in which air flow is even across all the pipes during operation. This is the result of avoiding stable points by mechanical trajectory design. As a result, even if the operation of the rotation tube is disturbed, it can continue to vibrate. There is a pneumatic tube connection hole in the lower part (fixed tube) of the actuator, into which air is injected to drive the actuator. This actuator is printed integrally using a 3D printer (Objet260 Connex3, Stratasys); thus, no assembly process is required for production. Because it is necessary to remove the support material after printing, the dimensions of each part must be designed appropriately. It is better to make the movable part and the fixed tube / rotation tube connecting part as narrow as possible to ensure improved operational stability and efficiency; thus, tweezers with a tip of 0.25 mm and a needle with a diameter of 0.5 mm were used for support removal. Therefore, the gap between the rotating part and the switching part was set to this size. The support material in the tube was first roughly removed with a long wire and then completely removed with a washing machine (LAC-RIM 3D, macoho) using a water stream. A summary of each actuator is provided in Table I.

B. Experimental equipment

The experimental apparatus used in this study is shown in Fig. 6 and the system configuration is shown in Fig. 7,

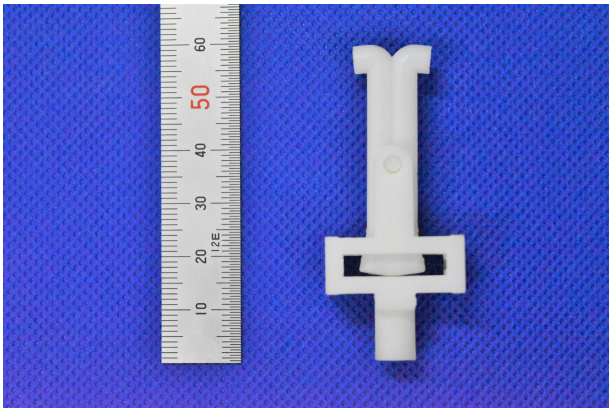

Fig. 4: Two-pipe model of the prototype actuator, which is the most basic actuator structure where self-excited vibration is induced and reciprocated by inflowing air (This is the model of $l = 20\,\mathrm{mm}$).

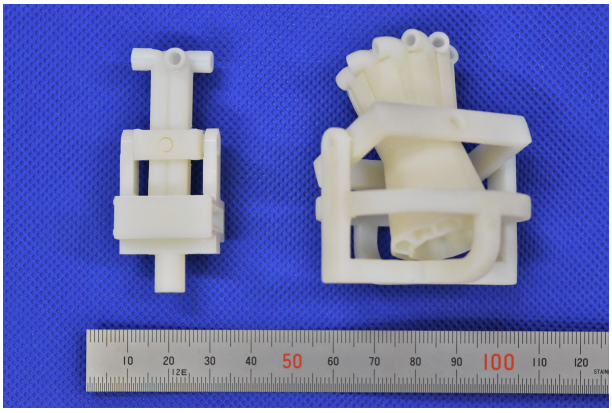

Fig. 5: 4-pipe and 10-pipe extensions of the actuator model shown in Fig. 4. By increasing the number of pipes, the motion displacement is increased and the stability is improved.

TABLE I: Overview of each actuator

Model	Mass [g]	Operating angle [deg]
2 pipes	4.4	±10 (Roll)
4 pipies	7.5	±10 (Both roll and pitch)
10 pipes	21.2	±25 (Both roll and pitch)

which simultaneously measured the actuator displacement and flow rate. This flow sensor can measure more than 40 m/s. In the experiment, the two-pipe actuator shown in Fig. 4 was used. An air compressor and an air tank were used as the air pressure source to maintain a sufficient pressure of 0.7 MPa. The flow rate of the compressed air obtained from the air pressure source was adjusted by the speed controller and flowed into the actuator. At this time, the flow rate of the air flowing through the actuator was measured using a flow sensor and divided by the cross-sectional area of the pipe to obtain the flow velocity value. In order to measure the operating frequency of the actuator in operation, the displacement was measured with a laser displacement meter at one point of the rotating tube, and the operating frequency was calculated from the data. Flow rate and displacement data were recorded with

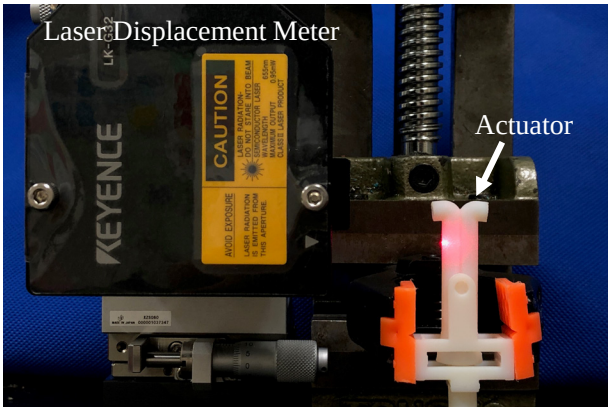

Fig. 6: Experimental equipment. Only the configuration for measuring the displacement of the actuator is shown. The displacement of one point of the rotating tube is measured by a laser displacement meter on the left side.

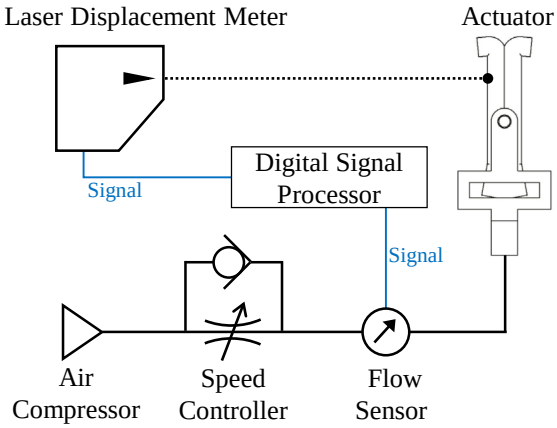

Fig. 7: System configuration of the experimental equipment.

a digital signal processor (DS1104, DSpace).

C. Results of motion experiments

The six models are shown in Table II with different gaps between the two tubes, l, and I. Air was introduced into the actuator and the operating frequency was measured. Fig. 9 shows the displacement of the actuator at the representative time obtained during the experiments. In the obtained waveform, the time passing through the center point was recorded and the frequency of each wave was obtained from the data. At the same time, the flow rate of air flowing into the actuator at each time was recorded. First, the gap between the fixed tube and the rotation tube does not significantly affect the operating frequency. Fig. 8 shows the operating frequency when air is input to Model A, Model B, and Model C. As a result, it was found that the gap does not affect the movement in the range of this experiment. However, the operating frequency of Model C is slightly higher under the high flow velocity, and it is expected that the efficiency is higher due to smaller air leakage. Fig. 10 shows the relationship between the resulting flow velocity and operating frequency with various values of

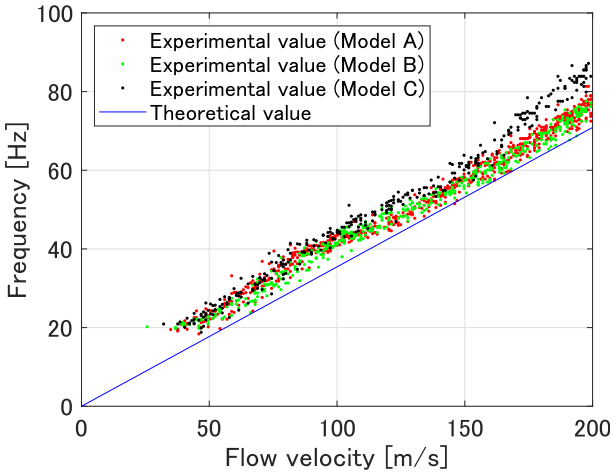

Fig. 8: Operating frequency when the gap is changed: It can be confirmed that the gap between the fixed tube and the rotation tube does not affect the operating frequency.

TABLE II: Actuator models with different gap between two tubes, l, and I.

	Gap [mm]	l [mm]	I [kg · m^2]
Model A	2.5	20	2.12×10^{-7}
Model B	1.5	20	2.12×10^{-7}
Model C	0.5	20	2.12×10^{-7}
Model D	0.5	30	4.05×10^{-7}
Model E	0.5	40	6.94×10^{-7}
Model F	0.5	40	10.2×10^{-7}

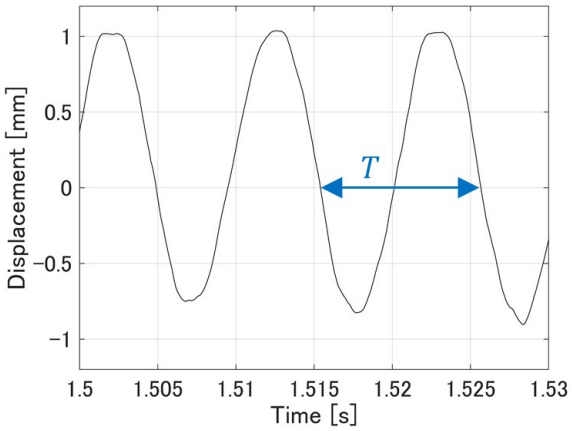

Fig. 9: Displacement at typical times. The operating frequency was calculated from the time passing through the center. The data are filtered by moving average with 50 samples.

l. Fig. 11 compares the operating frequency of different I with the same length of l to indicate the effect of momentum of inertia. Here, the theoretical values of the operating frequency were calculated by substituting the parameters of the actuator shown in Table II and Table III into Eq.(10) and are plotted in the same figure. The moment of inertia I of the rotating tube was calculated from a 3D CAD model. There is a difference between the experimental and theoretical values.

TABLE III: Parameters used to derive the theoretical values

A	7.07×10^{-6} m^2
ρ	1.296 kg/m^3

In the theoretical model, it was assumed that τ can be expressed by a linear function of the rotation angle θ. However, it is considered that the torque was not linear exactly at $-10^\circ < \theta < 10^\circ$. In experiments of some models, the operation stopped when the flow velocity dropped. This is because the torque generated by the air was sufficiently small with respect to the force due to friction between the rotating tube and the wall surface etc., and the vibration was attenuated. Comparing the Fig. 10 for changes in l, the larger l is, the lower the frequency. The larger l is, the smaller the variance of the data. This is because the moment of inertia has increased and the stability of the movement has improved. Comparing Fig. 11 for the change of I, as the theory shows, the larger the moment of inertia I, the lower the frequency. However, the torque was insufficient with respect to the moment of inertia, and operation stopped at a small flow rate.

The relationship between the flow velocity and the operating frequency was almost linear. This is the same as the result shown in Eq. (10), which was derived from the theoretical model. Thus, the theoretical model constructed in this study was valid.

V. Flapping Robot Application Example

In this section, we design a flapping robot using the theoretical model, and present the results of experiments using the robot to reveal the applicability of the proposed actuator to actual robots.

A. Robot design and development

In order to demonstrate the applicability of the proposed actuator, we built a prototype robot that flutters using the proposed actuator. The prototype robot is shown in Fig. 12. This robot is molded integrally with the actuator and has two wings on the arm extending from the rotating tube. The typical flapping frequency of insects is approximately 30 Hz; therefore, the wings were designed such that the operating frequency was the same. The wings were designed using Eq.(10) derived from the modeling of the actuator. The dimensions of the rotating tube were not changed from those used in the previous experiment ($l = 20$ mm); only the inertia moment I including the wing was adjusted. As a design procedure, the target moment of inertia, I, was determined from Eq.(10), and the calculated value on CAD including the moment of inertia of the blade was close to this value. At this time, the mass of the blade was assumed to be sufficiently large, and the fluid resistance due to flapping was ignored. The three parts of the robot (body, wings, and wing bones) were molded from resins with different Shore hardness values of 85 (Vero, Stratasys), 30 (Agilus 30, Stratasys), and 70 (mixing the two), respectively. The robot dimensions and material hardness values are shown in Fig. 13. The base of the wing has a movable range of $\pm 13^\circ$ (Fig. 14) and can rotate passively.

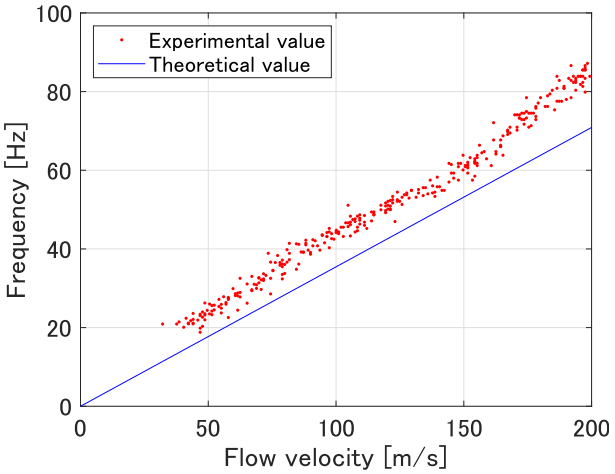

(a) Model C ($l = 20$ mm)

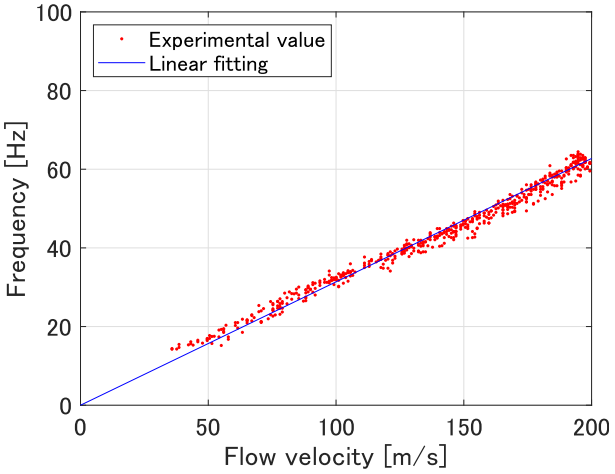

(b) Model D ($l = 30$ mm)

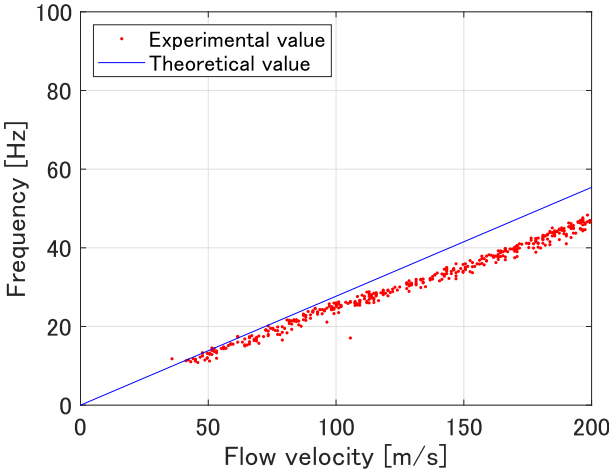

(c) Model E ($l = 40$ mm)

Fig. 10: Relationship between flow velocity and frequency (change l)

This robot was also printed integrally using a 3D printer such that it can be operated as a robot immediately after printing without any additional assembly process.

The actuator is driven by air flowing in from the bottom

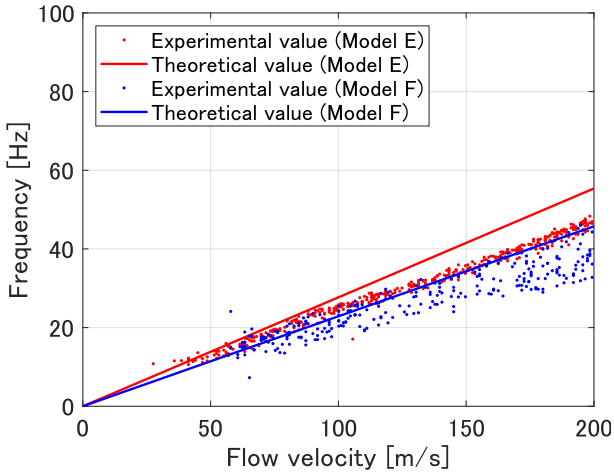

Fig. 11: Effect of moment of inertia on driving frequency. Model E: $I = 6.94 \times 10^{-7}$ [kg · m^2], Model F: $I = 10.2 \times 10^{-7}$ [kg · m^2]

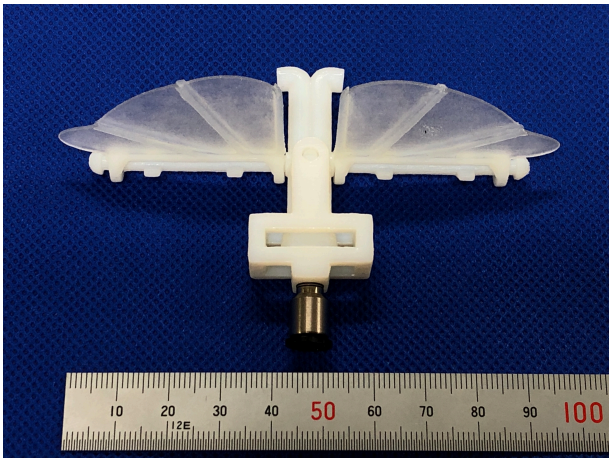

Fig. 12: Flapping robot with arms and wings attached to a two-pipe model actuator, which was integrally molded using a 3D printer.

of the robot and the mounted wings are shaken in antiphase. Propulsion is generated by vibration of the wings, which moves the robot forward.

B. Robot motion experiments

The experimental device shown in Fig. 15 was constructed for the robot motion experiment. The pneumatic tube was connected to the robot through a basic rotary joint, and the robot's own weight was supported by the tube. Propulsion was generated by the flapping motion of the robot so that the robot flew around the rotary joint.

When air was applied to the robot, it fluttered at approximately 25 Hz as designed and moved forward (Fig. 16). A model with the same shape and no wings was also made for comparison, revealing that the robot obtained thrust through the flapping motion generated by the actuator.

Thus, a pneumatic robot was easily and successfully manufactured by 3D printing using the proposed actuator. The

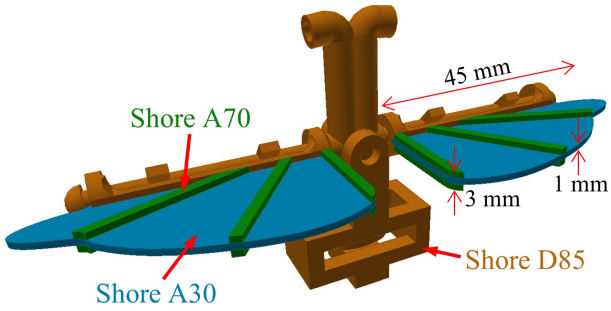

Fig. 13: Robot dimensions and material hardness values. Actuators, wings, and bones are all manufactured using materials with different hardness values.

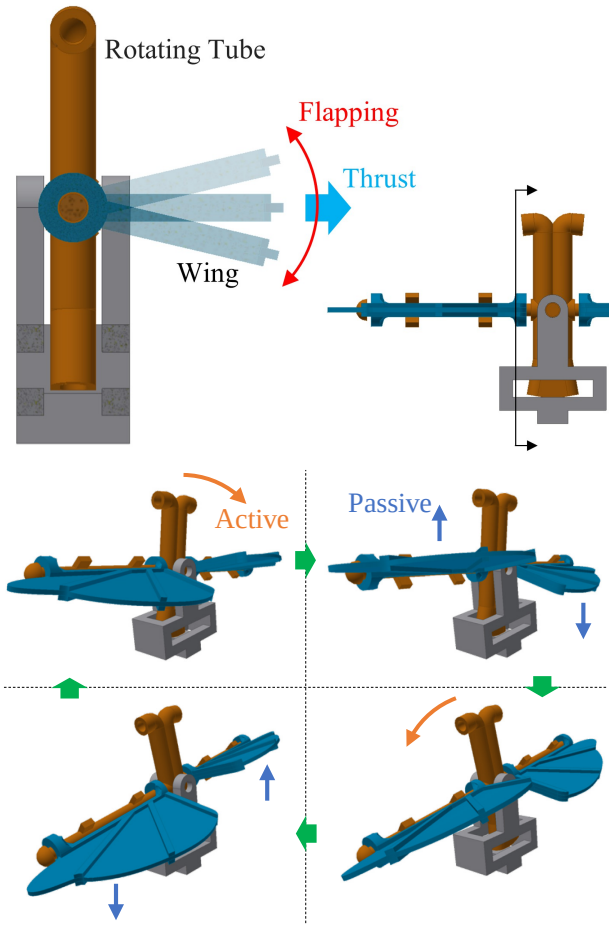

Fig. 14: Moving parts of the wing. A rotating joint was attached to the base of the wing to allow the wing to passively swing. The bottom figure shows the flapping motion, which is passively rotated by the vibration of the actuator.

actuator itself can be expanded as shown in Fig. 5; therefore, it is expected to have applications to various robots. Although there is a problem that the operation of the actuator becomes unstable due to the ejected air, it is believed that, in the future, its influence can be reduced by attaching a wall to the outlet of

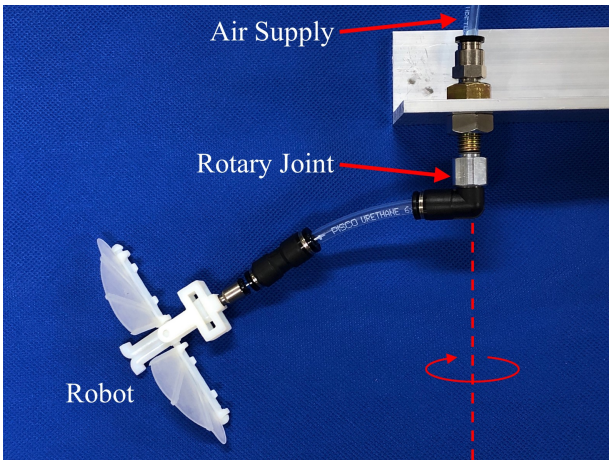

Fig. 15: Robot experimental setup. The pneumatic tube can be freely rotated by a rotary joint attached to the robot.

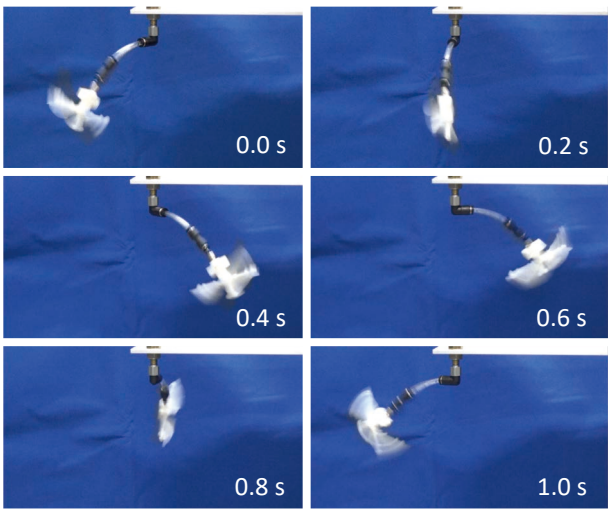

Fig. 16: Continuous photo of the flapping motion of the robot, which generates thrust and rotates.

the air. Also, applications that use jets, such as a pipe cleaning robot, will be studied in the future.

VI. CONCLUSIONS

In this study, we proposed and designed a pneumatic actuator that uses a flow path switching mechanism to induce self-excited vibration and that can be integrally molded with a 3D printer. This novel design simplifies manufacturing, driving, and control processes, thereby reducing the development costs of robots. The relationship between the flow velocity of the inflowing air and the operating frequency was clarified using a theoretical model of the two-pipe model , which forms the basic structure of the actuator, and validated through experiments on a prototype actuator. Experiments were also performed on a 4-pipe model and a 10-pipe model, which improved the stability of the prototype and increased the displacement. Finally, as an example of the application of actuators, we built a prototype robot that fluttered. Experiments revealed that this

actuator can be successfully applied to a pneumatic robot that can be easily manufactured by 3D printing. In the future, we will further demonstrate the applications of the actuator by performing independent operations using an air pressure source that can be mounted on the robot[33] and various other robot applications using an extended model of the actuator.

REFERENCES

[1] S. Tadokoro, *Overview of the ImPACT Tough Robotics Challenge and Strategy for Disruptive Innovation in Safety and Security*. Cham: Springer International Publishing, 2019, pp. 3–22.

[2] G. Dogangil, B. L. Davies, and F. R. y Baena, "A review of medical robotics for minimally invasive soft tissue surgery," *Proceedings of the Institution of Mechanical Engineers, Part H: Journal of Engineering in Medicine*, vol. 224, no. 5, pp. 653–679, 2010, pMID: 20718269. [Online]. Available: https://doi.org/10.1243/09544119JEIM591

[3] R. Niiyama, X. Sun, C. Sung, B. An, D. Rus, and S. Kim, "Pouch motors: Printable soft actuators integrated with computational design," *Soft Robotics*, vol. 2, no. 2, pp. 59–70, 2015. [Online]. Available: https://doi.org/10.1089/soro.2014.0023

[4] S. M. Felton, M. T. Tolley, C. D. Onal, D. Rus, and R. J. Wood, "Robot self-assembly by folding: A printed inchworm robot," in *2013 IEEE International Conference on Robotics and Automation*, May 2013, pp. 277–282.

[5] J. D. Carrico, K. J. Kim, and K. K. Leang, "3d-printed ionic polymer-metal composite soft crawling robot," in *2017 IEEE International Conference on Robotics and Automation (ICRA)*, May 2017, pp. 4313–4320.

[6] D. Drotman, S. Jadhav, M. Karimi, P. deZonia, and M. T. Tolley, "3d printed soft actuators for a legged robot capable of navigating unstructured terrain," in *2017 IEEE International Conference on Robotics and Automation (ICRA)*, May 2017, pp. 5532–5538.

[7] T. Umedachi and B. A. Trimmer, "Design of a 3d-printed soft robot with posture and steering control," in *2014 IEEE International Conference on Robotics and Automation (ICRA)*, May 2014, pp. 2874–2879.

[8] R. Niiyama, C. Rognon, and Y. Kuniyoshi, "Printable pneumatic artificial muscles for anatomy-based humanoid robots," in *2015 IEEE-RAS 15th International Conference on Humanoid Robots (Humanoids)*, Nov 2015, pp. 401–406.

[9] D. B. G. J. M.Wehner, R.L.Truby and R.J.Wood, "An integrated design and fabrication strategy for entirely soft, autonomous robots," vol. 536, pp. 451–455, 2016.

[10] R. MacCurdy, R. Katzschmann, Youbin Kim, and D. Rus, "Printable hydraulics: A method for fabricating robots by 3d co-printing solids and liquids," in *2016 IEEE International Conference on Robotics and Automation (ICRA)*, May 2016, pp. 3878–3885.

[11] A. L. Desbiens, Y. Chen, and R. J. Wood, "A wing characterization method for flapping-wing robotic insects," in *2013 IEEE/RSJ International Conference on Intelligent Robots and Systems*, Nov 2013, pp. 1367–1373.

[12] T. Li, G. Li, Y. Liang, T. Cheng, J. Dai, X. Yang, B. Liu, Z. Zeng, Z. Huang, Y. Luo, T. Xie, and W. Yang, "Fast-moving soft electronic fish," *Science Advances*, vol. 3, no. 4, 2017. [Online]. Available: https://advances.sciencemag.org/content/3/4/e1602045

[13] P. Li, Y. Wang, U. Gupta, J. Liu, L. Zhang, D. Du, C. C. Foo, J. Ouyang, and J. Zhu, "Transparent soft robots for effective camouflage," *Advanced Functional Materials*, vol. 29, no. 37, p. 1901908, 2019. [Online]. Available: https://onlinelibrary.wiley.com/doi/abs/10.1002/adfm.201901908

[14] H. Nabae and K. Ikeda, "Effect of elastic element on self-excited electrostatic actuator," *Sensors and Actuators A: Physical*, vol. 279, pp. 725 – 732, 2018. [Online]. Available: http://www.sciencedirect.com/science/article/pii/S092442471830709X

[15] T. Nemoto and A. Yamamoto, "Thermobot: A bipedal walker driven by constant heating," in *2015 IEEE/RSJ International Conference on Intelligent Robots and Systems (IROS)*, Sep. 2015, pp. 983–988.

[16] M. NAKASHIMA, N. OHGISHI, and K. ONO, "A study on the propulsive mechanism of a double jointed fish robot utilizing self-excitation control," *JSME International Journal Series C Mechanical Systems, Machine Elements and Manufacturing*, vol. 46, no. 3, pp. 982–990, 2003.

[17] J. Ute and K. Ono, "Fast and efficient locomotion of a snake robot based on self-excitation principle," in *7th International Workshop on Advanced Motion Control. Proceedings (Cat. No.02TH8623)*, July 2002, pp. 532–539.

[18] W. P. Weston-Dawkes, A. C. Ong, M. R. A. Majit, F. Joseph, and M. T. Tolley, "Towards rapid mechanical customization of cm-scale self-folding agents," in *2017 IEEE/RSJ International Conference on Intelligent Robots and Systems (IROS)*, Sep. 2017, pp. 4312–4318.

[19] D. Cunningham and H. H. Asada, "The winch-bot: A cable-suspended, under-actuated robot utilizing parametric self-excitation," in *2009 IEEE International Conference on Robotics and Automation*, May 2009, pp. 1844–1850.

[20] K. Ono, R. Takahashi, A. Imadu, and T. Shimada, "Self-excitation control for biped walking mechanism," in *Proceedings. 2000 IEEE/RSJ International Conference on Intelligent Robots and Systems (IROS 2000) (Cat. No.00CH37113)*, vol. 2, Oct 2000, pp. 1143–1148 vol.2.

[21] K. Ono, R. Takahashi, and T. Shimada, "Self-excited walking of a biped mechanism," *The International Journal of Robotics Research*, vol. 20, no. 12, pp. 953–966, 2001. [Online]. Available: https://doi.org/10.1177/02783640122068218

[22] S. Maeda, Y. Hara, T. Sakai, R. Yoshida, and S. Hashimoto, "Self-walking gel," *Advanced Materials*, vol. 19, no. 21, pp. 3480–3484, 2007. [Online]. Available: https://onlinelibrary.wiley.com/doi/abs/10.1002/adma.200700625

[23] Y. Miyaki and H. Tsukagoshi, "Soft simple compact valve inducing self-excited vibration aimed for mobile robots unnecessary for electricity," in *2018 IEEE/ASME International Conference on Advanced Intelligent Mechatronics (AIM)*, July 2018, pp. 670–675.

[24] T. Takayama and Y. Sumi, "Self-oscillated air flow passage changing device for bundled tube locomotive device," *Proceedings of the 2018 JSME Conference on Robotics and Mechatronics*, vol. 2016, pp. 2A2–08b2, 2016, in Japanese.

[25] D. Kim, J. I. Kim, and Y. Park, "A simple tripod mobile robot using soft membrane vibration actuators," *IEEE Robotics and Automation Letters*, vol. 4, no. 3, pp. 2289–2295, July 2019.

[26] Y. Iida and H. Tsukagoshi, "Compact valve inducing self-excited vibration and its applications," *Proceedings of the 2018 JSME Conference on Robotics and Mechatronics*, vol. 2019, pp. 1P1–K10, 2019, in Japanese.

[27] P. Rothemund, A. Ainla, L. Belding, D. J. Preston, S. Kurihara, Z. Suo, and G. M. Whitesides, "A soft, bistable valve for autonomous control of soft actuators," *Science Robotics*, vol. 3, no. 16, 2018. [Online]. Available: https://robotics.sciencemag.org/content/3/16/eaar7986

[28] K. Suzumori, A. Koga, and H. Riyoko, "Microfabrication of integrated fmas using stereo lithography," in *Proceedings IEEE Micro Electro Mechanical Systems An Investigation of Micro Structures, Sensors, Actuators, Machines and Robotic Systems*, Jan 1994, pp. 136–141.

[29] The Japan Fluid Power System Society, *Hydraulic and pneumatic handbook*. Ohmsha, Ltd., 1989, in Japanese.

[30] M. Harada and S. Ozaki, *Fluid particle engineering (in Japanese)*. Yokendo, 1969, in Japanese.

[31] R. Woszidlo, F. Ostermann, C. N. Nayeri, and C. O. Paschereit, "The time-resolved natural flow field of a fluidic oscillator," *Experiments in Fluids*, vol. 56, no. 6, p. 125, Jun 2015. [Online]. Available: https://doi.org/10.1007/s00348-015-1993-8

[32] J. Gregory and M. N. Tomac, "A review of fluidic oscillator development," in *43rd AIAA Fluid Dynamics Conference*, 2013, p. 2474.

[33] M. Wehner, M. Tolley, Y. Meng, Y.-L. Park, A. Mozeika, Y. Ding, C. Onal, R. Shepherd, G. Whitesides, and R. Wood, "Pneumatic energy sources for autonomous and wearable soft robotics," *Soft Robotics*, vol. 1, pp. 263–274, 12 2014.